Adaptive Wavelet Networks for Power-Quality Detection and Discrimination in a Power System

Chia-Hung Lin and Chia-Hao Wang

***Abstract*—This paper proposes a model of power-quality detection for power system disturbances using adaptive wavelet networks (AWNs). An AWN is a two-subnetwork architecture, consisting of the wavelet layer and adaptive probabilistic network. Morlet wavelets are used to extract the features from various disturbances, and an adaptive probabilistic network analyzes the meaningful features and performs discrimination tasks. AWN models are suitable for application in a dynamic environment, with add-in and delete-off features using automatic target adjustment and parameter tuning. The proposed AWN has been tested for the power-quality problems, including those caused by harmonics, voltage sag, voltage swell, and voltage interruption. Compared with conventional wavelet networks, the test results showed accurate discrimination, fast learning, good robustness, and faster processing time for detecting disturbing events.**

***Index Terms*—Adaptive probabilistic network, adaptive wavelet network (AWN), Morlet wavelet, power quality.**

I. Introduction

POWER quality has attracted considerable attention from both utilities and users due to the use of many types of sensitive electronic equipment, which can be affected by harmonics, voltage sag, voltage swell, and momentary interruptions. These disturbances cause problems, such as overheating, motor failures, inaccurate metering, and misoperation of protective equipment. Voltage swell and sag can occur due to lightning, capacitor switching, motor starting, nearby circuit faults, or accidents, and can also lead to power interruptions. Harmonic currents due to nonlinear loads throughout the network can also degrade the quality of services to sensitive high-tech customers, such as Taiwan's science parks in Xin-Zhu and Tai-Nan. Recently, the massive rapid transit system (MRT) and high-speed railway (HSR) have been rapidly developed, facilitated by the widespread use of semiconductor technologies in the autotraction systems. As a result, the harmonic distortion level has worsened due to these increased uses of electronic equipment and nonlinear loads. Ensuring power quality (PQ) as well as providing harmonic and voltage disturbance detection is then increasingly important.

To ensure PQ, a system must be able to monitor, locate, and classify disturbances by measurement approaches and instruments. These instruments must collect large amounts of measured data such as voltages, currents, and occurrence times. However, they do not automatically classify disturbances and they require offline analysis from the recorded data. Fast Fourier transformation (FFT) has been applied to steady-state phenomenon but short-time duration disturbances require short-time Fourier transformers (STFTs) to aid the analysis. The choices for size of the time window affect both the frequency and time resolution when using STFT. In order to improve these limitations, wavelet theory [1] has been applied to model several short-term events. It thus allows for the convenient reconstruction of short duration with a tool to examine the effects of the short-term transient effects on the power system. For this, a method based on wavelet transformation (WT) for PQ analysis has been presented [2]. This method combines the use of the continuous wavelet transform (CWT) and its modulus maxima properties together with the multiresolution signal decomposition and reconstruction by means of the discrete-time wavelet transform (DTWT).

Wavelet networks (WNs) were initially designed to classify different types of disturbances [3], [4]. With multiresolution and localization of the wavelets [5] and pattern recognition capability of the artificial neural network (ANN), WNs have become important for signal and pattern analysis. However, ANNs have some drawbacks, including the determination of the network architecture and network parameters assignment. When networks are applied in dynamic environments, especially for online applications, traditional networks can become the bottleneck in adaptive applications. Accordingly adaptation methods, such as probabilistic and general regression neural networks, have been presented [6]–[8] and are recognized as having an expandable or reducible network structure, fast learning speed, and promising results. In these adaptation methods, the choice of smoothing parameter has significant effects on the network outcome, and the parameter is usually based on the overall statistical calculation from precollected training data. However, this approach may not be suitable to apply in a dynamical modeling environment, since the model needs to change pattern nodes with add-in or delete-off features. Therefore, a dynamic model needs a nonstatistical method as well as automatic adjustment of the targets and smoothing parameters for dynamic process technique [10].

In this paper, an integrated model of the adaptive wavelet network (AWN) is proposed to discriminate PQ disturbances, including harmonic and voltage fluctuation phenomena, by combining the Morlet wavelet and adaptive probabilistic network. AWN consists of two subnetworks connected in cascade. In the wavelet layer, the activation functions take the Morlet wavelets and are responsible for extracting features from unknown signals. Following the probabilistic network is an adaptive network

Manuscript received December 27, 2004; revised December 21, 2005. Paper no. TPWRD-00625-2004.

The authors are with the Department of Electrical Engineering, Kao-Yuan University, Kaohsiung 821, Taiwan, R.O.C. (e-mail: eechl53@educities.edu.tw).

Digital Object Identifier 10.1109/TPWRD.2006.874105

with automatic parameters for tuning and performing the discrimination task. A sample power system is presented here as an example, and computer simulations show computational efficiency, fast learning, accurate discrimination, and good robustness for different tests.

II. Adaptive Wavelet Network (AWN)

A. Morlet Wavelet

In applications of signal analysis, it is necessary to extract signal features with Fourier transformation, but it is only a time-domain transform, which has no time-frequency localization features. Fourier analysis consists of breaking up a signal into sinusoidal waves of various frequencies. Similarly, wavelet analysis is the breaking up of a signal into dilations and translation versions of the original wavelet, referred to as the mother wavelet. The wavelets must be oscillatory, have amplitudes that quickly decay to zero, and have at least one vanishing moment. The Morlet wavelet is the modulated Gaussian function, so this family is built starting from the following complex Gaussian function [9]:

$$\psi(x) = \left(e^{j\omega_o x} - e^{-\frac{\omega_o^2}{2}}\right) e^{-\frac{x^2}{2\sigma}}, \quad \sigma > 0. \tag{1}$$

The Fourier transform of $\psi(x)$ is

$$\hat{\psi}(\omega) = \sqrt{2\pi\sigma}\left[e^{\frac{-(\omega-\omega_o)^2}{2\sigma}} - e^{-\frac{\omega_o^2}{2}} e^{-\frac{\omega^2}{2\sigma}}\right]. \tag{2}$$

According to (2), suppose $\omega = 0$, then $\hat{\psi}(0) = 0$, that is $\int_R \psi(x)dx = 0$, which represents the collection of all measurable functions in the real space, and $\psi(x)$ satisfies the admissibility condition. When $\omega_0 \geq 5$, then the Morlet wavelet becomes

$$\begin{aligned}\varphi(x) &= e^{j\omega_o x} e^{-\frac{x^2}{2\sigma}} = [\cos(\omega_o x) + j\sin(\omega_o x)]\, e^{-\frac{x^2}{2\sigma}} \\ &= \varphi_R(x) + j\varphi_I(x), \quad \omega_0 \geq 5,\ \sigma > 0\end{aligned} \tag{3}$$

where $\varphi_R(x)$ and $\varphi_I(x)$ are the real and imaginary part, respectively. The function of $\varphi(x)$ is also an appropriate admissible wavelet. When $\varphi(x) \in L^2(R)$, then $\varphi(x)$ becomes the mother wavelet with dilation parameter d and translation parameter t

$$\varphi_{d,t}(x) = \varphi_{R_{d,t}}\left(\frac{x-t}{d}\right) + j\varphi_{I_{d,t}}\left(\frac{x-t}{d}\right), \quad d \in R \setminus \{0\},\ t \in R$$

$$\begin{cases} \varphi_{R_{d,t}}\left(\frac{x-t}{d}\right) = \cos\left[\frac{5(x-t)}{d}\right] e^{-\frac{(x-t)^2}{2\sigma d^2}} \\ \varphi_{I_{d,t}}\left(\frac{x-t}{d}\right) = \sin\left[\frac{5(x-t)}{d}\right] e^{-\frac{(x-t)^2}{2\sigma d^2}} \end{cases}. \tag{4}$$

By adjusting the parameters d and t, the formulas $\varphi_{Rd,t}(x)$ and $\varphi_{Id,t}(x)$ have localization performance in both time and frequency. Fig. 1 shows the wavelets with various dilation parameters ($d = 1, 2, 3$) and translation parameters ($t = -1, 0, 1$). In this paper, both real and imaginary parts of the $\varphi_{d,t}(x)$ are used to extract features from the unknown signals $\varphi_{Rd,t}(x)$ in order to extract the features of harmonic and voltage fluctuation phenomena in preliminary analysis. They are similarly applied to $\varphi_{Id,t}(x)$ in order to extract the features of the disturbances, including harmonics, voltage sags, voltage swells, sags or swells involving harmonics, and momentary interruptions in detailed analysis. Therefore, the activation functions of the wavelet nodes are derived from the mother wavelet $\varphi_{di,ti}(x_i)$ for $i = 1, 2, 3, \ldots, n$, where n is the number of the wavelet nodes. The input vector $X = [x_1, x_2, \ldots, x_i, \ldots, x_n]$ is connected to the wavelet network, and inputs are the sample data from the distorted wave as shown in Fig. 2.

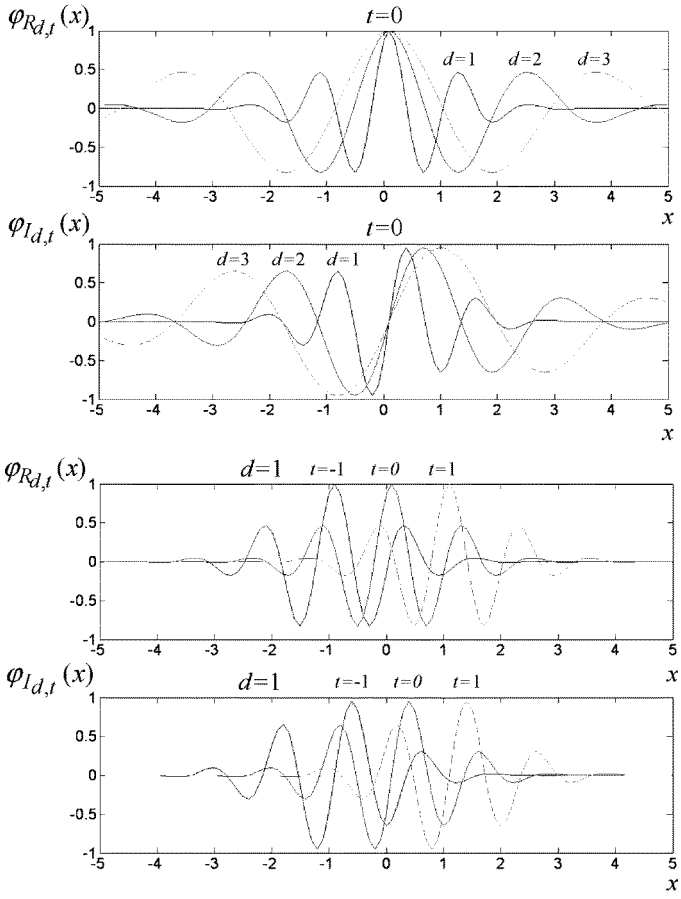

Fig. 1. Wavelets with various dilations and translations.

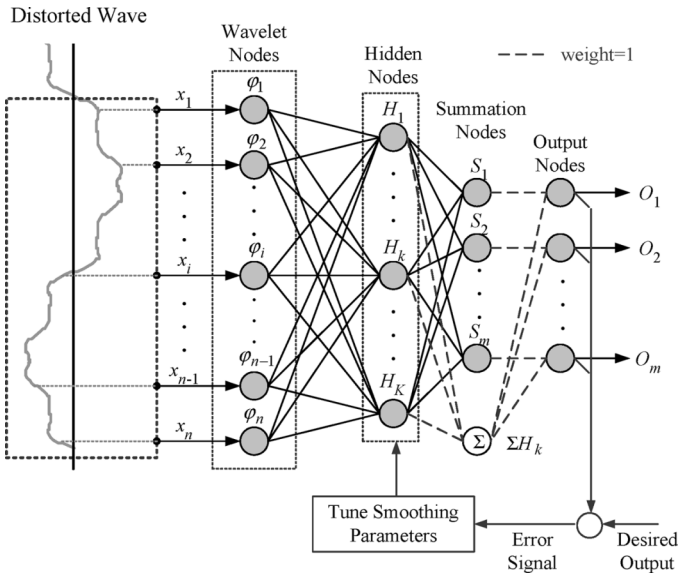

Fig. 2. Architecture of the AWN.

B. Adaptive Probabilistic Network

In this paper, an integrated wavelet network is proposed to discriminate PQ disturbances, and this network combines the properties of the Morlet wavelets with the advantages of probabilistic network [6]–[8]. The second subnetwork with a hidden, summation, and output layer is shown in Fig. 2. The number of hidden nodes $H_k(k = 1, 2, 3, \ldots, K)$ is equal to the number of training examples, while the number of summation nodes S_j and output nodes $O_j(j = 1, 2, 3, \ldots, m)$ is equal to the types of disturbances. The weights w_{ki}^{WH} (connecting the kth hidden node and the ith wavelet node) and w_{jk}^{HS} (connecting the jth summation node and the kth hidden node) are determined by K input–output training pairs. The final output of node O_j is [7]

$$H_k = \exp\left[-\sum_{k=1}^{K} \frac{\left(\varphi_i(x_i) - w_{ki}^{WH}\right)^2}{2\sigma_k^2}\right] \tag{5}$$

$$O_j(\varphi) = \frac{\sum_{k=1}^{K} w_{jk}^{HS} H_k}{\sum_{k=1}^{K} H_k} = \frac{s(\varphi)}{h(\varphi)}. \tag{6}$$

However, there are no means of generating an optimal σ_k, and adjusting the σ_k would refine the discrimination accuracy in the dynamic environment. The optimal σ_k is intended to minimize the predicted squared error function e_j [10], which is defined as

$$e_j(\varphi, T) = [T_j - O_j(\varphi)]^2 \tag{7}$$

where T_j is the desired output for input vector X. The first partial derivatives of error are shown in (8)

$$\begin{aligned}\frac{-\partial e_j(\varphi, T)}{\partial \sigma_k} &= 2\left[T_j - O_j(\varphi)\right]\frac{\partial O_j(\varphi)}{\partial \sigma_k} \\ &= 2\left[T_j - O_j(\varphi)\right]\left[\frac{\frac{\partial s(\varphi)}{\partial \sigma_k} - O_j(\varphi)\frac{\partial h(\varphi)}{\partial \sigma_k}}{h(\varphi)}\right] \\ \begin{cases} \frac{\partial s(\varphi)}{\partial \sigma_k} = 2\left[\sum_{k=1}^{K} w_{jk}^{HS} H_k\right]\left[\frac{\left(\varphi_i(x_i) - w_{ki}^{WH}\right)^2}{2\sigma_k^3}\right] \\ \frac{\partial h(\varphi)}{\partial \sigma_k} = 2\left[\sum_{k=1}^{K} H_k\right]\left[\frac{\left(\varphi_i(x_i) - w_{ki}^{WH}\right)^2}{2\sigma_k^3}\right] \end{cases}.\end{aligned} \tag{8}$$

The parameter σ_k is then updated by using pattern learning, as in (9)

$$\sigma_k(p+1) = \sigma_k(p) + \eta\frac{\partial e_j(\varphi, T)}{\partial \sigma_k} \tag{9}$$

where η is the learning rate, and p is the iteration number. The algorithm of the AWN contains two stages: the learning stage and recalling stage, as detailed below.

Learning Stage:

Step 1) For each training example $X(k) = [x_1(k), x_2(k), \ldots, x_i(k), \ldots, x_n(k)]$ for $k = 1, 2, 3, \ldots, K$ and $i = 1, 2, 3, \ldots, n$, create weights w_{ki}^{WH} between wavelet node φ_i and hidden node H_k by

$$\varphi_i(k) = \sin\left[\frac{5\left(x_i(k) - t_i\right)}{d_i}\right] e^{-\frac{\left(x_i(k) - t_i\right)^2}{2\sigma d_i^2}} \tag{10}$$

$$x_i = V(nT), \quad t_i = V_c(nT)$$

$$w_{ki}^{WH} = \varphi_i(k) \tag{11}$$

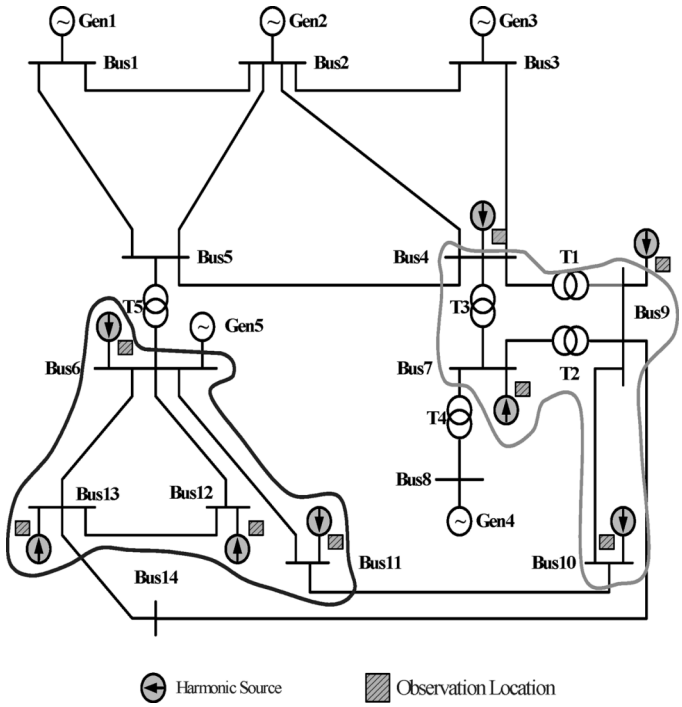

Fig. 3. One-line diagram of the 14-bus power system.

where d_i is the dilation parameter $d_i \in Z$; x_i is a sequence of samples obtained from an unknown signal V; t_i is the translation parameter, a sequence of samples obtained from fundamental wave V_c in the time domain; n is the number of sampling points; T is the sampling period; and $W^{WH} = [w_{ki}^{WH}]$ is a k by n matrix.

Step 2) Create weights w_{jk}^{HS} between hidden node H_k and summation node O_j by

$$w_{jk}^{HS} = \begin{cases} 1 & (j = 1, 2, 3, \ldots, m) \\ 0 \end{cases} \tag{12}$$

where the values of w_{jk}^{HS} are the predicted outputs associated with each stored pattern w_{ki}^{WH}, and $W^{HS} = [w_{jk}^{HS}]$ is the k by m matrix. Connection weights from hidden nodes H_k to summation node Σ are set to 1.

Recalling Stage:

Step 1) Get network weights w_{ki}^{WH} and w_{jk}^{HS}.

Step 2) Apply test vector $X = [x_1, x_2, x_3, \ldots, x_i, \ldots, x_n]$ to the AWN. Compute the output of wavelet node φ_i

$$\varphi_i(x_i) = \sin\left[\frac{5(x_i - t_i)}{d_i}\right] e^{-\frac{(x_i - t_i)^2}{2\sigma d_i^2}}. \tag{13}$$

Step 3) Compute the output of hidden node H_k by the Gaussian activation function

$$H_k = \exp\left[-\sum_{k=1}^{K} \frac{\left(\varphi_i(x_i) - w_{ki}^{WH}\right)^2}{2\sigma^2}\right] \tag{14}$$

where $\sigma_1 = \sigma_2 = \ldots = \sigma_k = \ldots = \sigma_K = \sigma$, the optimal value can be obtained by using (8) and (9) based on the minimum misclassification error.

Step 4) Compute the outputs of node O_j by using (6).

TABLE I
HARMONIC CURRENT COMPONENTS IN PERCENTAGE BY FIELD TESTS

Bus Bar	3rd	5th	7th	9th	11th	13th	15th	17th	19th	21th	23rd	25th	Non-linear Device
7, 11, 13	1.50	22.0	15.0	0.00	10.2	8.40	0.00	4.30	3.40	0.00	0.59	0.00	6-pulse rectifier
4, 6	0.15	0.55	0.29	0.00	6.20	4.50	0.00	0.10	0.21	0.00	0.46	0.00	12-pulse rectifier
9	0.00	17.0	10.1	0.00	6.10	4.42	0.00	3.83	3.20	0.00	2.58	2.32	Static frequency converter
10	13.8	5.05	2.59	1.57	1.05	0.75	0.57	0.44	0.35	0.29	0.24	0.20	Thyristor-controlled reactor
12	1.20	33.6	1.60	0.00	8.70	1.20	0.00	4.50	1.30	0.00	2.80	0.00	DC Motor

III. DISTURBANCE EVENTS DETECTION SYSTEM (DEDS)

A. Training Patterns Creation

In this paper, disturbance events [11] are considered, including harmonics, voltage sag and swell, and momentary interruptions. Harmonic currents and voltages are caused mostly by electronic equipment, and harmonic events may occur over a long duration. Voltage sag may be caused by the switching operations, starting large motor loads, and nearby circuit faults. Voltage sags may drop down to 70% of the nominal result due to heavy load switching or fault conditions with a duration up to 0.5 s. Long duration voltage sags down to 80% of the nominal value have a typical duration up to 10 s. Voltage swells may occur when large loads are removed from the system and when a single-phase fault occurs in the distribution part of the system. Interruptions are typically the result of occurrence and subsequent clearing of faults in the distribution portion of the system, and the voltage magnitude is always less than 10% of the nominal voltage. These events are caused by faults, equipment failures, and control malfunctions. A total interruption could be tolerated by the protection equipment for up to 20 ms.

A 14-bus system is used for the test example, as shown in Fig. 3 [12]. The system has five generator buses, 15 lines, five transformers, and eight nonlinear devices. The buses with harmonic sources are the buses used to take measurements for observation, and there are eight observation locations in this system. At each observation location, harmonic and voltage fluctuation phenomena are considered, as well as the harmonic source causing voltage distortion for neighboring buses. Table I shows the harmonic current components as percentages of each harmonic source by the field test. With harmonic power flow [13], we can simulate harmonic voltages at selected observation locations. We can also consider various harmonic load combinations and work durations at each observation location (i.e., combinations {Bus13}, {Bus13,Bus6}, {Bus13,Bus11}, {Bus13,Bus12}, {Bus13,Bus6,Bus11}, {Bus13,Bus6,Bus12}, {Bus13,Bus11,Bus12} at Bus13). In addition, we can determine voltage fluctuations including sags, swells, sags or swells involving harmonics, and voltage interruptions. Training data can be systematically collected at Bus13 with input/output pairs training data. Each input is conducted within the period of sampling data from distorted waves. The four sample rates f_S we consider are 1.44, 2.88, 5.76, and 11.52 kHz, and the number of sample points n_S are 24, 48, 96, and 192. Equation (10) with sequencing preprocess is applied on various distorted waves for extraction features. The wavelet layer eliminates the 60-Hz sinusoid components, and the remaining components are reconstructed by the n wavelet nodes to form the WT patterns. The various WT patterns reveal

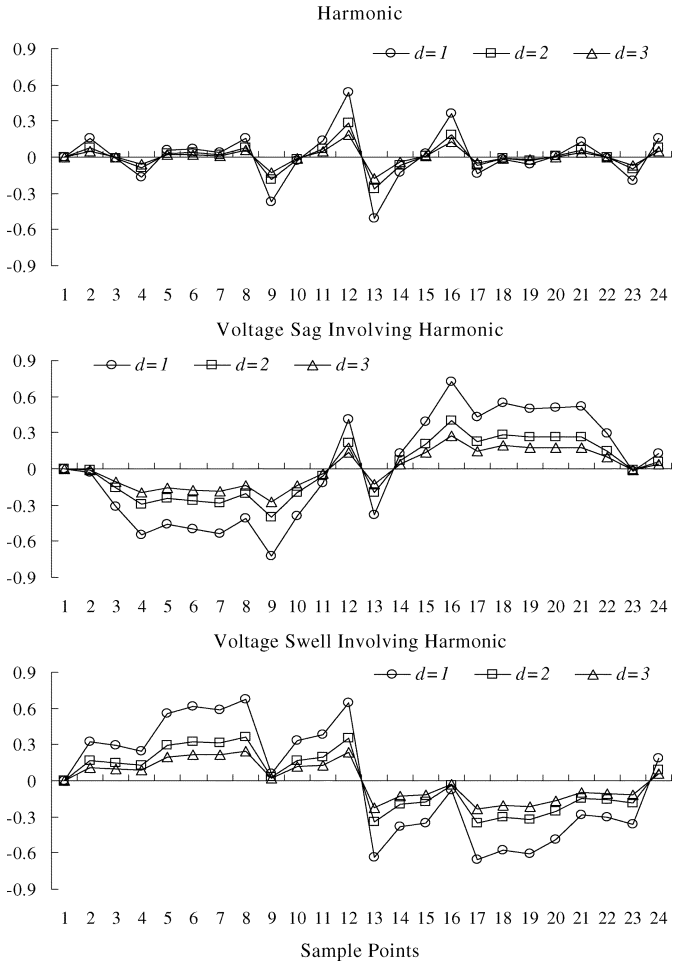

Fig. 4. WT patterns with various dilations and a sampling rate of 1.44 KHz.

the rise or dip characteristics for voltage fluctuation, and the sawtooth characteristics for harmonic fluctuation. For example, Fig. 4 has dilations $d = 1, 2, 3$ and shows the WT patterns with sample rates 1.44 kHz at observation location Bus13.

According to the various patterns, the weights between wavelet nodes and hidden nodes are determined by training data. The weights between hidden nodes and summation nodes are the predicted outputs associated with each input pattern by encoding signal "1" for "Abnormal", and "0" for "Normal." At each observation location, we have the following events as:

- normal: the pattern is [0000];
- harmonics: the pattern is [1000];
- voltage sag: the pattern is [0100];
- voltage swell: the pattern is [0010];
- voltage interruption: the pattern is [0001];
- voltage sag involving harmonic: the pattern is [1100];
- voltage swell involving harmonic: the pattern is [1010].

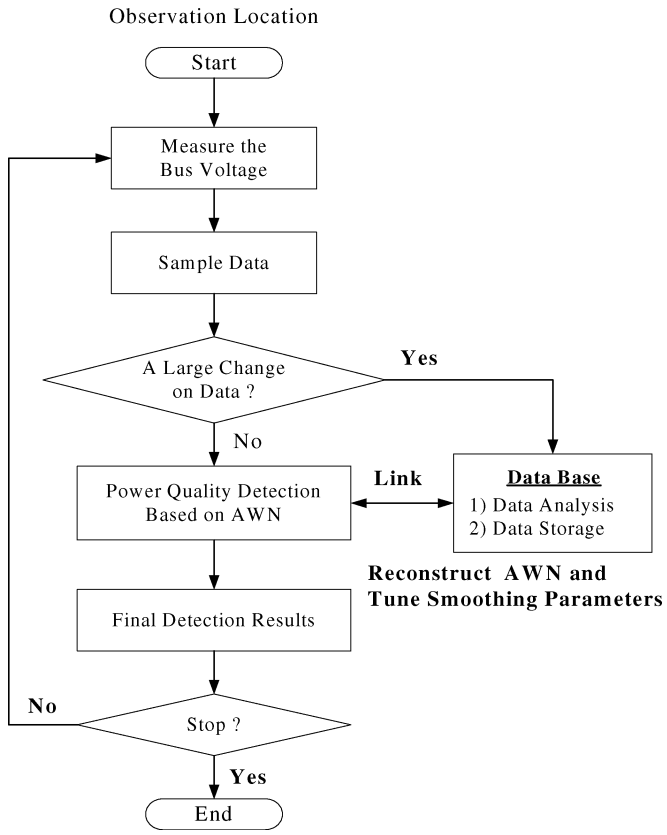

Fig. 5. Flowchart of the DEDS at each observation location.

B. Flowchart of the DEDS

The flowchart of the proposed DEDS is shown in Fig. 5. At each observation location (Loc-4, Loc-6, Loc-7, Loc-9, Loc-10, Loc-11, Loc-12, and Loc-13), bus voltage records are taken from the SCADA interface and each full cycle of a distorted wave is used for detection by AWN. The amplitude signals $(x_1, x_2, \ldots, x_i, \ldots, x_n)$ from distorted waves are sequentially input to the AWN (AWN-4, AWN-6, AWN-7, AWN-9, AWN-10, AWN-11, AWN-12, and AWN-13). When the periodic sampling data are provided, find the buses with total harmonic voltage distortion $V_{\mathrm{THD}} \geq 2.5\%$. If sampling data with voltages varying due to great load changes (half- or over-load), such as the changes of harmonic components or the ranges of voltage magnitude, learning data can be continually formed for the data update to the current database. In a real power system, learning data could be periodically collected by a portable recording device placed at observation location [14]. The new learning sets of data are presented to the AWN, including new features or events, the corresponding patterns nodes will continue to grow, and use (10), (11), and (12) to create the network weights without reiteration to corrupt the previous database or structure. This process results in very fast training, and the network is adaptive to data changes by tuning smoothing parameters. After the learning stage is finished, the proposed AWN can still work in a new operating mode. In power quality detection (PQD), the wavelet layer is used to extract the features, and the features will be reconstructed for various patterns. The following probabilistic network is responsible for the final discrimination of the disturbance events. Output vector $\mathrm{O} = [O_1, O_2, O_3, O_4]$ is evaluated by the AWN, and a threshold value 0.5 is designed for element O_j ($j = 1, 2, 3, 4$) to separate normal from abnormal values. The output values are between 0 and 1, where a value close to 1 means "Normal," 0 means "Abnormal," and O_j then indicates the possible disturbing events at the observation location.

TABLE II
RELATED PARAMETERS SETTING OF THE AWN

Model	Network Topology				Training Patterns K	Ranges of Dilation d	Learning Rate η
	W	H	S	O			
*I	24	55	5	4	55	(0 3]	(0 1]
II	48	55	5	4			
III	96	55	5	4			
IV	192	55	5	4			

Note: W-H-S-O: Wavelet-Hidden-Summation-Output Node.

IV. SIMULATION RESULTS AND DISCUSSION

In a 14-bus system, most harmonics are related to power rectifiers or converters with harmonic current components in percentages as shown in Table I. With fundamental and harmonic power flow for various loading combinations, bus voltages can be calculated. At each observing location, we have a 55 set of training data for the AWN with the following events:

- harmonics: harmonic load combinations with seven sets of training data $K_{\mathrm{har}} = 7$;
- voltage sag or sag involving harmonics: voltage reduction between 10∼30% in magnitude with 22 sets of training data $K_{\mathrm{sag}} = 22$;
- voltage swell or swell involving harmonics: voltage rise between 10∼30% in magnitude with 22 sets of training data $K_{\mathrm{swell}} = 22$;
- voltage interruption: voltage magnitude less than 10% of nominal with three sets of training data $K_{\mathrm{int}} = 3$;
- normal: normal sinusoid wave with 1 set of training data $K_{\mathrm{nor}} = 1$.

In this paper, DEDS was used to monitor eight locations for detection disturbances. According to the four types of sampling rates, four models of the AWN are proposed, as shown in Table II. For comparison purposes, we have also applied the WBPN composed of n Morlet wavelets in the wavelet layer and conventional neural network. For the second subnetwork, a back-propagation neural network (BPN) is used for training with the back-propagation learning algorithm. Only one hidden layer is used, and the number of hidden nodes is determined by the experience formulas [15]. The DEDS was designed on a PC Pentium-IV 2.4 GHz with 480-MB random-access memory (RAM) and Matlab software. To show the effectiveness of the proposed DEDS, three case studies are chosen for demonstration.

A. Learning Performance Tests

With Model I, Fig. 6(a) and (b) show the smoothing parameters and squared errors versus learning cycles, respectively. The discrimination performance of the AWN is affected by the width of the Gaussian activation function. As the width of Gaussian

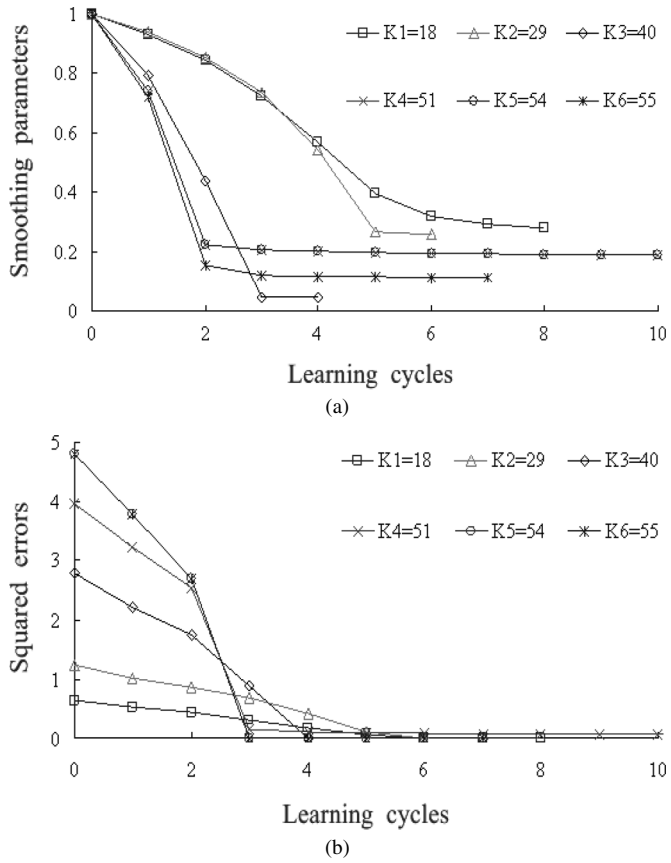

Fig. 6. (a) Smoothing parameters versus learning cycles. (b) Squared errors versus learning cycles.

TABLE III
COMPARISON OF AWN WITH WBPN

Method	Network Topology	Training Patterns	Learning Rate η	Learning Cycles	Average CPU Time (s)	Confident Value
*AWN	24-55-5-4	55	0.2	≤10	0.625	>0.95
WBPN	24-24-14-4	55	0.2	<8000	<600	0.80~0.90
			0.5			
			0.8			

function decreases, decision boundaries can become increasingly nonlinear. For a very narrow Gaussian function, the network approaches a nearest-neighbor classifier. Equations (8) and (9) are used to find near-optimum smoothing parameters that minimize the training-data error of the AWN as the number of training data increases from K1 = 18 to K6 = 55. The corresponding hidden nodes will continue to grow from 18 to 55, and construct the network weights without any iteration process. This process results in very fast training, and the network is adaptive to change patterns with add-in (or delete-off) features by tuning smoothing parameters for six learning stages. Fig. 6(b) shows the final squared errors after the training AWN has been responsible for determining the smoothing parameters. For squared error $e = 10^{-3}$, the proposed method rapidly converges to the nearest local minimum for less than ten learning cycles in a shorter processing time.

Table III compares the learning performance of the AWN and WBPN. Subnetwork BPN weights and learning rates η were determined by a tedious and trial-and-error procedure. Learning

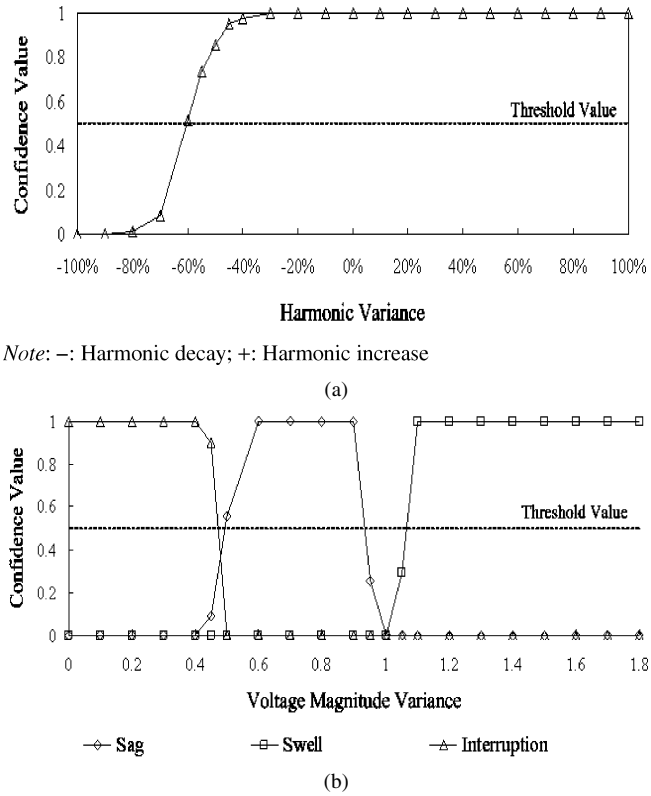

Note: −: Harmonic decay; +: Harmonic increase

Fig. 7. (a) Detection confidence versus harmonic variant. (b) Detection confidence versus voltage magnitude variant.

rates $\eta = 0.2$, 0.5, and 0.8 were selected for training. With various tests, we can see that the training time of AWN substantially outperformed WBPN. The detection confidence of AWN is higher than the WBPN. Although the AWN topology is slightly greater than WBPN, AWN has a fast learning process that does not need any iteration for updating weights, a flexible hidden nodes mechanism with add-in or delete-off, and automatic adjustment of the targets and parameter σ. With the same training data, the proposed AWN shows better performance than WBPN.

B. Discrimination Performance Test

To test the robustness of the proposed method in the operating mode, testing data (never presented to the training data) were produced with harmonic voltages varying from −100% to +100% and voltage magnitudes varying from 0 to 1.8 p.u. at the Loc-13, where symbol "+" means harmonic increase and symbol "−" means harmonic decay due to load changes. Fig. 7(a) shows the confidence value versus the harmonic variant with average output values for seven trained data and 154 untrained data. The test shows that the proposed method has the high detection confidence for harmonic voltages variances upon −60% by using the threshold value of 0.5. Fig. 7(b) shows the confidence value versus voltage magnitude variance with average output values for 47 trained data and 107 untrained data including sag, sag involving harmonics, swell, swell involving harmonics, and voltage interruption. With training data for "voltage sag" having a specific sag range between 0.7 and 0.9 p.u., voltage magnitudes between 0.50 and 0.95 p.u. were strongly identified as "sag events" by using the threshold

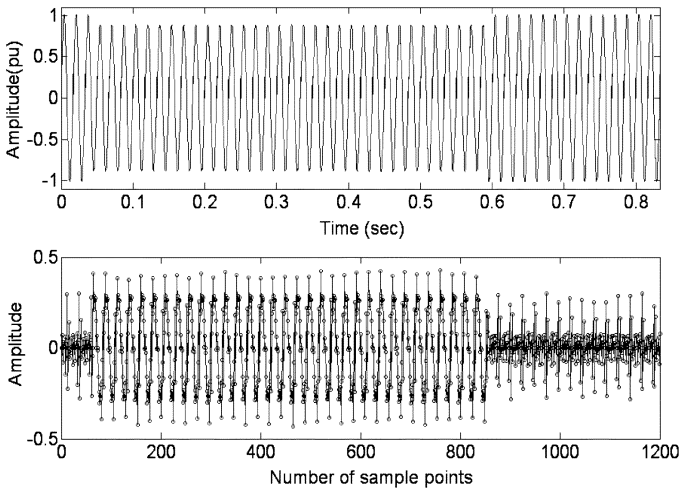

Fig. 8. Time-domain wave and WT patterns at Bus12.

value of 0.5. The same results can be also observed for "voltage swells" between 1.05 and 1.8 p.u. Voltage interruption was gradually identified with the voltage magnitude of less than 0.45 p.u.

In the computer simulation for changing traced disturbances, testing data were produced with data-varying voltage magnitudes and harmonic components; and then Gaussian noises were added randomly with zero mean and $\pm 10\%$ variance. With only 48 or 55 training data, the proposed method can work in an environment with load changes, magnitude variances, and data with noise influence. The test confirms that the proposed method has a better capability for enhancing the discrimination performance.

C. Case Study—Multiple Harmonics and Voltage Sag Involving Harmonics

Eight observation locations were used, as shown in Fig. 3. With fundamental and harmonic power flow, we can simulate bus voltages at observation locations. Time-domain analysis was conducted to detect the distorted waves with 50 cycles (about 0.8 s). Periodic sampling was done with sampling rate $f_S = 1.44$ kHz and sample points $n_S = 24$. With multiple harmonic sources at Bus6, Bus9, Bus12, and Bus13, sampled data were then applied to each AWN (AWN-6, AWN-9, AWN-12, AWN-13) for detection. For example, let the voltage sags caused by heavy motor loads at Bus12, and multiple harmonic sources be at Bus6, Bus9, and Bus13. Fig. 8 shows the waves of voltage sag within about 30 cycles. When the voltage sag suddenly reaches 12%, periodic sampling is then performed. The wavelet layer reconstructs the voltage features to WT patterns as shown in Fig. 8. WT patterns show the times for starting and ending of occurrences, show characteristics of harmonics in normal work duration, and extract the compound characteristics of voltage sag involving harmonics of about 30 cycles. AWNs can monitor the overall duration including the beginning and ending cycles. For 50 detection cycles, Fig. 9 shows the detection results at Bus6, Bus9, Bus12, and Bus13. This confirms that the proposed models have a higher confidence value of detection results in the tests.

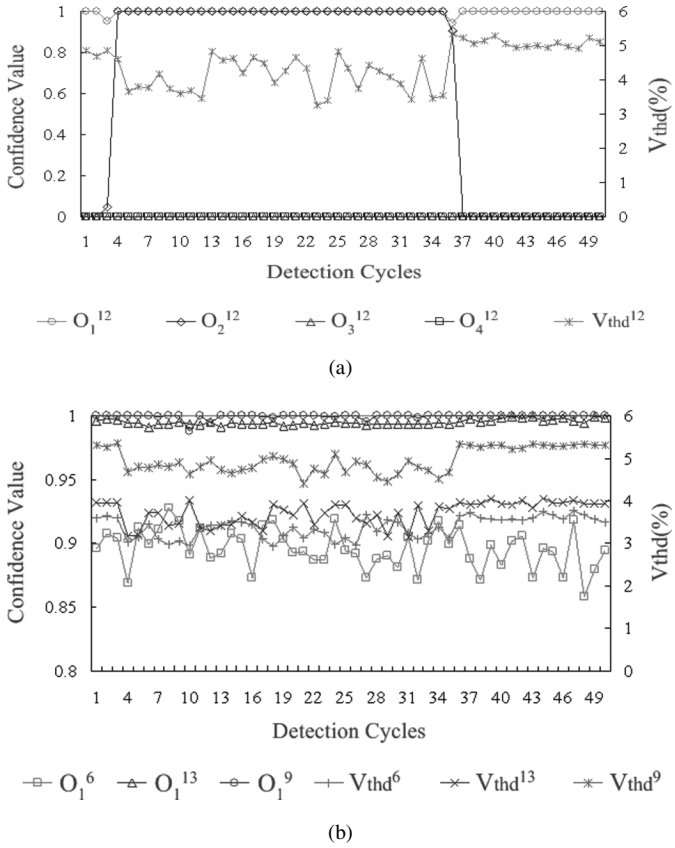

Fig. 9. (a) Detection results at Bus12. (b) Detection results at Bus6, Bus13, and Bus9.

V. Conclusion

The disturbance event detection system with AWNs has been developed in this paper. AWN combines the use of Morlet wavelets and adaptive probabilistic networks for discriminating PQ disturbances including harmonics and voltage fluctuation phenomena. The proposed AWN model has a dynamic and fast adaptation algorithm with continuity add-in or delete-off features by automatically tuning the targets and smoothing parameters of hidden nodes. Some advantages of the AWNs are:

- the training processes are very fast compared with other multilayer wavelet networks;
- the network architecture can be built using adaptive training algorithms, and can avoid the determination of network weights by the trial-and-error procedure;
- by enhancing the particular features of disturbance events, the proposed method is able to improve the discrimination performance;
- AWN has good detection accuracy, good robustness, and classification performance;
- DEDS with AWNs can simultaneously monitor PQ at each observation location.

Computer simulation shows that DEDS could be very effective to detect PQ disturbances. For a well-dispatched power system, this concept will be used in a real-time and an offline analysis tool, and SCADA/EMS will be integrated without extra devices.

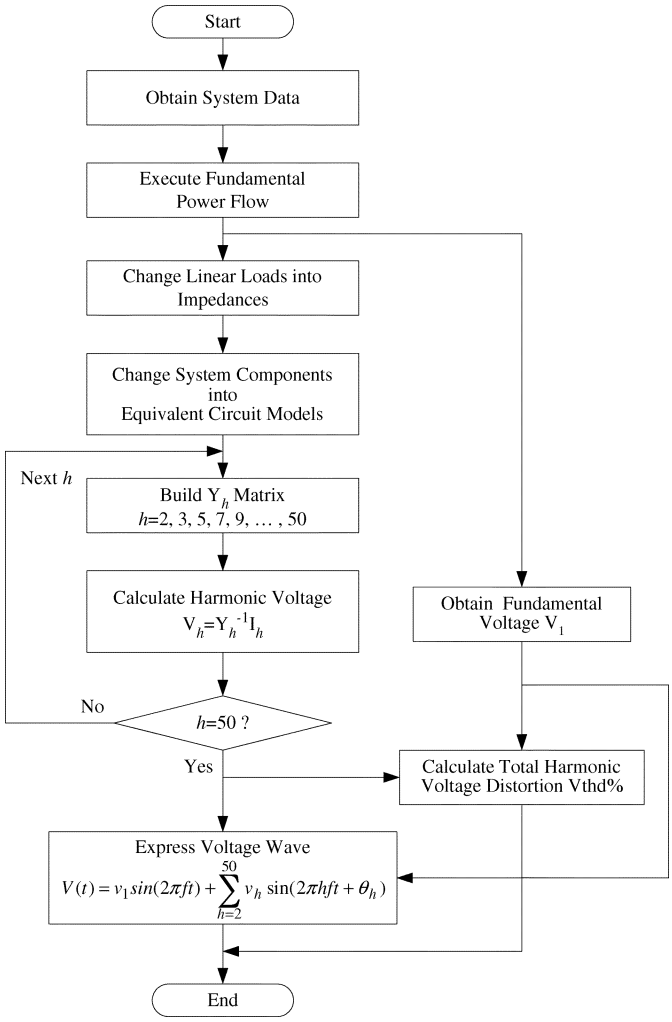

Fig. 10. Flowchart of harmonic power flow.

APPENDIX

Harmonic power-flow models [13] were used in this paper. Transmission lines were modeled as pi-equivalent circuits; transformers were considered as simplified series resistances and reactances; shunt magnetizing components were ignored; and the leakage inductances were assumed to be constant. Capacitors were considered constant with impedances varying with frequencies. The generators were series impedances of resistance and reactance for fundamental load flow. For harmonic load-flow analysis, generators were modeled as subtransient reactances. Linear loads were represented as series impedances of resistance and reactance. Nonlinear loads were treated as harmonic current sources. Harmonic current components were used by field record data. The flowchart of harmonic power-flow analysis developed in this paper is shown in Fig. 10.

ACKNOWLEDGMENT

The authors would like to thank the associate editor and the reviewers for reviewing the manuscript and providing suggestions.

REFERENCES

[1] P. Pillay and A. Bhattacharjee, "Application of wavelet to model short-term power system disturbances," *IEEE Trans. Power Syst.*, vol. 1, no. 4, pp. 2031–2037, Nov. 1996.
[2] L. Angrisani, P. Daponte, M. D'Apuzzo, and A. Testa, "A measurement method based on the wavelet transform for power quality analysis," *IEEE Trans. Power Del.*, vol. 13, no. 4, pp. 990–998, Oct. 1998.
[3] S. Santoso, E. J. Powers, and W. M. Grady, "Power quality disturbance identification using wavelet transforms and artificial neural networks," in *Proc. IEEE Int. Conf. Harmonics and Quality of Power*, Las Vegas, NV, Oct. 16–18, 1996, pp. 615–618.
[4] L. Angrisani, P. Daponte, and M. D'Apuzzo, "Wavelet network-based detection and classification of transients," *IEEE Trans. Instrum. Meas.*, vol. 50, no. 5, pp. 1425–1435, Oct. 2001.
[5] Y.-C. Huang, "A new data mining approach to dissolved gas analysis of oil-insulated power appatatus," *IEEE Trans. Power Del.*, vol. 18, no. 4, pp. 1257–1261, Oct. 2003.
[6] D. F. Specht and H. Romsdahl, "Experience with adaptive probabilistic and general regression neural networks," in *Proc. IEEE World Congr. Computational Intelligence*, vol. 2, Orlando, FL, 1994, pp. 1203–1208.
[7] W.-M. Lin, C.-H. Lin, and Z.-C. Sun, "Adaptive multiple fault detection and alarm processing for loop system with probabilistic network," *IEEE Trans. Power Del.*, vol. 19, no. 1, pp. 64–69, Jan. 2004.
[8] Z.-C. Mo and W. Kinsner, "Probabilistic neural networks for power line fault classification," in *Proc. IEEE Canadian Conf. Electrical and Computer Engineering*, vol. 2, May 24–28, 1998, pp. 585–588.
[9] L. C. Chun and Q. Zhengding, "A method based morlet wavelet for extracting vibration signal envelope," in *Proc. 5th Int. Conf. on Signal Processing WCCC-ICSP*, vol. 1, Aug. 21–25, 2000, pp. 337–340.
[10] T. L. Seng, M. Khalid, and R. Tusof, "Adaptive GRNN for the modeling of dynamic plants," in *Proc. IEEE Int. Symp. Intelligent Control*, Vancouver, BC, Canada, Oct. 27–30, 2002, pp. 217–222.
[11] *IEEE Recommended Practices for Monitoring Electric Power Quality*, ANSI/IEEE Std. 1159-1995.
[12] C.-H. Wu and C.-R. Chen, "Apply artificial neural network to power system in detecting the positions of the harmonic sources," in *Proc. 21st Symp. Electrical Power Engineering*, Taiwan, R.O.C., Nov. 2000, pp. 329–333.
[13] Y. H. Yan, C. S. Chen, C. S. Moo, and C. T. Hsu, "Harmonic analysis for industrial customer," *IEEE Trans. Power Del.*, vol. 30, no. 2, pp. 462–468, Mar./Apr. 1994.
[14] C.-H. Lin and M.-C. Tsao, "Power quality detection with classification enhancible wavelet-probabilistic network in a power system," *Proc. Inst. Elect. Eng., Gen., Transm. Distrib.*, vol. 152, no. 6, pp. 969–976, Nov. 2005.
[15] Y.-Y. Hong and Y.-C. Chen, "Application of algorithms and artificial-intelligence approach for locating multiple harmonics in distribution system," *Proc. Inst. Elect. Eng., Gen., Transm. Distrib.*, vol. 146, no. 3, pp. 325–329, May 1999.

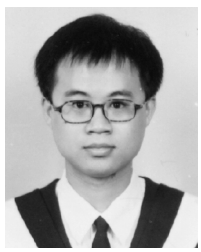

Chia-Hung Lin was born in 1974. He received the B.S. degree in electrical engineering from the Tatung Institute of Technology, Taipei, Taiwan, R.O.C., in 1998, and the M.S. and Ph.D. degrees in electrical engineering from the National Sun Yat-Sen University, Kaohsiung, in 2000 and 2004, respectively.

Currently, he is the Assistant Professor in the Department of Electrical Engineering, Kao-Yuan University, Kaohsiung, where has been since 2004. His research interests include fault diagnosis in power systems, neural-network computing, and harmonic analysis. His current interests are biomedical signal processing and analysis.

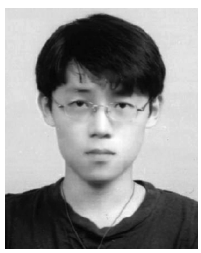

Chia-Hao Wang was born in 1981. He received the B.S. degree in electrical engineering from the Chin-Yi Institute of Technology, Tai-zhong, Taiwan, R.O.C., in 2003, and the M.S. degree in electrical engineering from the National Sun Yat-Sen University, Kaohsiung, in 2005.

His research interests include neural-network computing, harmonic analysis, and digital circuit design.